12-15-2019

Utility of Bench Scale Sand Tank Experiments at Assessing Permeable Reactive Barrier Design

Brandon Meier

UTILITY OF BENCH SCALE SAND TANK EXPERIMENTS AT ASSESSING PERMEABLE REACTIVE BARRIER DESIGN

By

Brandon E. Meier

Bachelor of Science – Geology
University of Nevada, Las Vegas
2015

A thesis submitted in partial fulfillment
of the requirements for the

Master of Science – Geology

Department of Geoscience
College of Sciences
The Graduate College

University of Nevada, Las Vegas
December 2019

UNLV | GRADUATE COLLEGE

Thesis Approval

The Graduate College
The University of Nevada, Las Vegas

October 18, 2019

This thesis prepared by

Brandon E. Meier

entitled

Utility of Bench Scale Sand Tank Experiments at Assessing Permeable Reactive Barrier Design

is approved in partial fulfillment of the requirements for the degree of

Master of Science – Geology
Department of Geoscience

Michael Nicholl, Ph.D.
Examination Committee Chair

Kathryn Hausbeck Korgan, Ph.D.
Graduate College Dean

Markus Berli, Ph.D.
Examination Committee Member

David Kreamer, Ph.D.
Examination Committee Member

Jacimaria Batista, Ph.D.
Graduate College Faculty Representative

Abstract

The objective of this work was to evaluate the utility of bench scale sand tank experiments at assessing permeable reactive barrier (PRB) design. Our criteria for meeting this goal was that differences between PRB designs could be identified solely by measuring concentration in outflow from the sand tank models. For our PRB designs (funnel-and-gate, staggered wells, and parallel bars), numerical simulations clearly showed that PRB design had a quantifiable effect on outflow concentration, provided that the solute reacted with the PRB materials. Conversely, use of a conservative (non-reactive) solute did not allow us to discern between PRB design alternatives. Employing the data collected from the numerical simulations can refine the design of the reactive barriers prior to physical sand tank experiments. Utilization of numerically simulated reactive barriers could be a way to predict and validate the use of a physical, bench-scale sand tank models.

Table of Contents

Abstract iii

List of Tables x

List of Figures xi

Section 1: Introduction 1

Section 2: Physical Experiments 3

Section 3: Simulation of the Physical Experiments 6

Section 4: Conceptualization 9

Section 5: Results 12

Section 6: Discussion 15

Conclusions 21

Appendix A: Tables 22

Appendix B: Figures 24

References 29

Curriculum Vitae 31

List of Tables

Table 1: Material parameters. 22

Table 2: Finite Element statistics for each PRB configuration. 22

Table 3: Simulation Matrix. 22

Table 4: Hydraulic Head (cm) at the outflow node 23

Table 5: Cumulative solute recovery at the final time step (480 hours) for the non-reactive simulations. 23

Table 6: Cumulative solute recovery at the final time step (2960 hours) for the reactive simulations. 23

List of Figures

Figure 1: Map view of three PRB configurations 24

Figure 2: Bench-scale sand tank experiment with supporting apparatus. 24

Figure 3: Calibrated numerical simulations 25

Figure 4: Vector velocity map 25

Figure 5: Map view of the simulation domains 26

Figure 6: Model results for non-reactive simulations as a function of mass fraction. 27

Figure 7: Model results for Q1 (2.1 mL/min) as a function of cumulative outflow mass. 27

Figure 8: Model results for Q2 (3.22 mL/min) as a function of cumulative outflow mass. 27

Figure 9: Model results for Q3 (5.0 mL/min) as a function of cumulative outflow mass. 27

Section 1: Introduction

The term Permeable Reactive Barrier (PRB) refers to a widely used technology for passive remediation of shallow (<30 m) groundwater systems (Blowes et al., 1998). In this approach, a selective barrier is installed in the subsurface at a location where the natural flow system will cause the contaminated groundwater to pass through the treatment materials (e.g., Obiri-Nyarko et al., 2014). The PRB is then expected to operate 24/7 in virtually any weather condition, and with minimal operational costs for power, maintenance, or staffing (e.g., Jeen et al., 2011). The success of a PRB-based remediation approach is highly dependent on carefully matching the design (e.g., location, size, shape, configuration, treatment materials) to site-specific conditions (e.g., Gavaskar et al., 1999). In addition to extensive site characterization (e.g., Day et al., 1999), the design process typically involves some combination of: laboratory batch and/or column tests (e.g., Kebria et al., 2016; Kornilovych et al., 2018), pilot-scale field experiments (e.g., Vogan et al., 1999; Weisener et al., 2005), and full-scale numerical simulations (e.g., Mayer et al., 2001).

Bench-scale sand tank experiments may provide a cost-effective means for testing PRB designs (e.g., Luo et al., 2016). Batch and column tests are used to evaluate treatment materials (e.g., Krüger et al., 2012), but do not allow direct comparison between design alternatives (e.g., size, shape, configuration). Field tests are expensive and time consuming (e.g., Jeen et al., 2011; Kornilovych et al., 2018; Vogan et al., 1999), which severely restricts the number of scenarios that can be considered. Numerical simulations readily allow comparison between alternative PRB designs (e.g., Gavaskar et al., 1999), but do not incorporate the full flow/chemical complexity found in field applications. In contrast, bench-scale sand tank models allow testing PRB designs under simulated field conditions. Sand tank experiments can be designed to

incorporate site-specific characteristics, such as: porous media, hydraulics, hydrochemistry, and biota (e.g., Ursino et al., 2001; Truax et al., 1995). The main drawbacks of using sand tanks are: expense, volume of waste generated, time required, and non-intrusive data collection (MJ Nicholl personal communication).

Here, numerical simulations are employed to consider the utility of sand box experiments for the purpose of evaluating PRB design. We assume a bench-scale sand tank as the basis for comparing the performance of the three different PRB configurations shown in Figure 1: funnel-and-gate (e.g., Higgins et al., 2009), passive wells (e.g., Hudak et al., 2008), and parallel bars (e.g., Obiri-Nyarko et al., 2014). For each configuration, flow and reactive transport are simulated in the two-dimensional horizontal plane using Hydrus 2D/3D (Simunek et al., 2011). All simulation parameters (dimensions, boundary conditions, material properties, duration, sampling approach, etc.) are based on lessons learned from a physical sand tank experiment. Simulation results show that non-intrusive measurement of outflow concentration from a sand tank experiment would allow effective comparison between these three designs for a reactive tracer, but not for a conservative (non-reactive) tracer.

Section 2: Physical Experiments

A bench-scale sand tank model was fabricated to compare the effectiveness of two reactive materials for remediation of groundwater contaminated with hexavalent chromium, Cr(VI). The tank was designed with a funnel-and-gate PRB containing either: 1) Granular Activated Carbon (GAC); or 2) a newly developed variant of GAC called Activated Carbon coated in Polysulfide Rubber (AC-PSR). The GAC was chosen because it is widely used for remediation of both metals and organic compounds (Babel et al., 2003; Li et al., 2002). The AC-PSR was developed to improve the performance of GAC for metal absorption and has proven effective in laboratory batch tests (Mortazavian, et al., 2019). To focus on the efficacy of the reactive materials, the sand tank was designed to minimize competing effects. Flow was restricted to the two-dimensional horizontal plane by installing a homogeneous, isotropic, and chemically inert analog aquifer with no internal sensors or wires. All measurements of solute concentration were made non-intrusively by sampling the system outflow.

An 85.1 x 17.6 x 25.0 cm (Length, Width, Height) analog aquifer was installed in a tank constructed from ½" thick acrylic sheet (Figure 2). The washed medium sand used to construct the analog aquifer had a measured hydraulic conductivity of 0.02 cm/s and porosity of 0.44. A funnel-and-gate design (Figure 1A) was employed to focus all flow through a 1.0 x 2.0 x 24.0 cm (LWH) filter pack holding the reactive material (GAC or AC-PSR). Hydraulic conductivity and porosity of the reactive materials were measured to be 0.076 cm/s and 0.60, respectively. Eight 1-cm diameter fully penetrating wells were installed in the aquifer; four upstream and four downstream of the funnel-and-gate (Figure 2). The upstream reservoir was held at a depth of 20 cm to establish a constant head boundary at the upstream end of the aquifer. Flow was induced by using a peristaltic pump set to extract water from the downstream reservoir at a rate of 1.5

liters per 24 hours (1.04 mL/min) for Exp. 01 (GAC) and 1.0 liters per 24 hours (0.70 mL/min) for Exp. 02 (AC-PSR). Experiments were started by injecting 100 mL of Cr(VI) solution (1000 mg/L) across the full depth of the analog aquifer. The injection well was centrally located 5 cm down-gradient from the upstream constant head boundary and 35 cm up-gradient from the PRB. The accumulated outflow was collected at 24-hour intervals; temperature and pH were measured before collecting subsamples for subsequent measurement of Cr(VI) concentration. The tank and all internal components, including the analog aquifer were either sanitized or replaced between the two trials.

In Exp. 01 (GAC), Cr(VI) was first measured on the 5th day post injection and continued a steep rise (Figure 3) until the concentration peaked on day 8 (175 hours). In Exp. 02 (AC-PSR), Cr(VI) was first measured on the 7th day post injection and peaked on day 10 (225 hours). Results from Exp. 01 and Exp. 02 showed that 66% and 81% of the injected Cr(VI) passed through the system over the experimental duration, respectively. Exp. 01 was intended to capture the sorption characteristics, but was of insufficient duration to provide data on desorption. Exp. 02 displayed an asymmetric concentration curve that flattens near the end of the experiment, signifying that discharge of Cr(VI) would have likely continued for an unknown time due to slow desorption from the AC-PSR (*Kinetics of Water-Rock Interaction*, 2008). Differing flow rates (GAC 1.04 mL/min, AC-PSR 0.70 mL/min) and test durations (GAC 9 days, AC-PSR 23 days) complicated comparison between the two reactive materials (Figure 3). After correcting for the differing flow rates, the data from Exp. 01 and Exp. 02 were too similar to distinguish between the two. As a result, we were unable to assess the performance of the materials based solely on the sand tank experiments. This result conflicted with expectations from laboratory batch and column experiments that indicated a 10-fold increase of absorption of the AC-PSR

over the GAC (Mortazavian, et al., 2019). As a substitute, calibrated numerical simulations were used to further interrogate system behavior.

Section 3: Simulation of the Physical Experiments

Flow and transport processes were simulated in the two-dimensional horizontal plane using HYDRUS 2D/3D (Simunek et al., 2011). This Galerkin linear finite-element model employs the Richards Equation to describe unsaturated-saturated flow in porous media and is also capable of simulating the movement of water vapor, heat, and multiple solutes. The model domain is discretized into a collection of 3-sided, near equilateral polygons, each of which is represented by a set of element equations that approximate the complex partial differential equations for flow (e.g., The Finite Element Method, 1980). At each time step, the element equations are combined in matrix form, and linked to appropriate boundary conditions. An iterative approach is used to estimate hydraulic head at the vertices of each polygon (nodes) by minimizing the residuals. The head field is then combined with the porous media properties for each polygon to produce velocity vectors at the nodes. The velocity field serves as the basis for calculating solute transport using a Fickian-based advection-dispersion equation. A number of sub-models are available to describe chemical interactions between the solutes, liquid water, and porous media (e.g., Simunek et al., 2011).

The physical experiments described above were simulated in Hydrus 2D/3D under fully saturated conditions in the 2D horizontal plane (M.J. Nicholl personal communication). The model domain closely matched the physical model in terms of dimensions, boundary/initial conditions, and media properties (hydraulic conductivity, porosity); sorption characteristics of the reactive media in the PRB (GAC, AC-PSR) were used for calibration. The upstream reservoir was replaced with a constant head boundary, while the downstream reservoir was explicitly modeled as a low-velocity mixing zone of high conductivity and porosity with a centrally located extraction node. A physical non-equilibrium model for sorption/desorption (M.J. Nicholl

personal communication) was matched heuristically to the results of the physical experiments (Figure 3). Conceptually, the pore water is divided into mobile (f_m) and immobile (f_i) fractions ($f_m + f_i = 1$). Immobile water resides in dead-end pores or is in close proximity to the pore walls, while the mobile water flows between connected pore spaces. Solute in the immobile water fraction is assumed to instantly absorb onto reactive material following a linear isotherm that is parameterized by the distribution coefficient (K_d). Conversely, solute in mobile water does not adhere ($K_d = 0$). A diffusion coefficient (α) describes solute transfer between the mobile and immobile water fractions.

In contrast to the physical experiments, the model outcomes allowed us to clearly discern between the two reactive materials. Results from the calibrated simulations (Figure 3) suggest a higher adsorption capacity for the AC-PSR ($K_d = 300$ cm^3/mg) than for the GAC ($K_d = 100$ cm^3/mg). This result conflicts with the laboratory equilibrium tests that predicted that AC-PSR would be an order of magnitude more effective at Cr(VI) removal than GAC. This discrepancy is most likely due to the much longer contact times of the batch experiments (48-hr) compared to the shorter contact times displayed in the physical experiments (20 seconds). The model calibration estimated that the fraction of immobile water (f_i) was 0.7 for the GAC and 0.1 for the AC-PSR. This result suggests that coating the particles with polysulfide rubber decreased the surface area of the individual particles (M.J. Nicholl personal communication).

In addition to providing estimates for the sorption properties of the test materials, the simulations showed that measurable amounts of solute were moving along slow flow paths on the downstream end of the funnel-and-gate. Velocity maps displayed a slight countercurrent on the downstream side of the funnel-and-gate resulting in no flow zones behind the funnel sections (Figure 4). Solute diffuses into these dead zones from the high concentration centroid of the

plume as it passes. These dead zones continued to release solute long after the concentration peak has passed which extended the tail of the outflow concentration curves. This result is an undesirable artifact of our experimental design that could have been avoided if the funnel-and-gate had not been sealed to the tank walls.

Section 4: Conceptualization

As discussed above, measurement of outflow concentration in a physical sand tank experiment did not provide sufficient information to discern between two different adsorptive materials that were deployed in identical aquifer/PRB configurations (Figure 3). Here, numerical simulations are used to determine if the outflow concentration from a physical sand tank model could be used to compare the effectiveness of three different PRB designs (Figure 1). In a funnel-and-gate design (Figure 1A), flow is directed into a narrow PRB by impermeable walls. This design provides a means to address widespread contamination, or plumes with multiple focal points (e.g., Higgins et al., 2009). Staggered rows of non-pumping wells backfilled with reactive material and constructed perpendicular to the flow path of a contaminant plume (Figure 1B) can be used where trench excavation is problematic (e.g., Hudak et al., 2008). A parallel bar design (Figure 1C) could be utilized in low conductivity sediments to avoid restricting the natural flow system (Obiri-Nyarko et al., 2014). Both the staggered well and parallel bar configurations require reactive materials that are significantly more permeable than the surrounding sediments so that flow is diverted into the treatment materials, rather than around them (Blowes et al., 1998).

The hypothetical bench-scale sand tank considered here is based on outcomes from the physical experiment described above (Figures 2 and 3). The tank width was effectively doubled (external dimensions of 100 x 40 x 25 cm, LWH) in order to allow flow to go around a 27 cm wide treatment zone; i.e., ~2/3 of the tank width for treatment and 1/3 to control lateral boundary effects. Steady-state flow through the system would be controlled by 5 cm thick fluid reservoirs at each end of the tank. To produce a small (<0.01 m/m) hydraulic gradient, the upstream reservoir would be held at a constant head, and fluid would be extracted from the center of the

downstream reservoir at a constant rate. Materials in the analog aquifer between the reservoirs would be readily available, homogenous, isotropic, and sufficiently permeable to avoid large head gradients. The tank design restricts flow vectors to the horizontal plane, which allows for high-resolution two-dimensional simulations. The downstream reservoir would be treated as a homogenous isotropic porous media of 100% porosity. To avoid the creation of unknown heterogeneities, including preferential flow paths and or local barriers, no sampling ports on sensors would be installed within the tank; data collection is restricted to measurement of solute concentration in the outflow stream.

Allowing for width of the tank walls (i.e., 1/2" thick acrylic plate), and replacing the upstream reservoir with a constant head boundary produces a horizontal model domain of 92.46 x 37.46 cm. To facilitate direct comparison between the three PRB designs under consideration (Figure 5), each was configured to have the same amount of reactive material, overall width, and longitudinal distance from the contaminant source. The area covered by the reactive material (113.04 cm^2) is not an integer number because it is easier to set precise dimensions for rectangles (Figure 5A, 5C) than circles (Figure 5B). The leading edge of each PRB is located 47.73 cm from the upstream reservoir, and 37.73 cm downstream from the solute injection point. The finite element mesh for each PRB configuration was generated automatically; mesh statistics are shown in Table 2. Initial conditions, including the solute pulse concentration (100 mg/cm^3), pulse duration (0.1 hours), test duration (20 days for nonreactive, 123 days for reactive simulations), and porous media properties (Table 1) were equal across all simulations. Boundary conditions, including constant upstream hydraulic head, constant outflow via extraction node, and no-flux side walls were consistent across all simulations as well. For simplicity, we considered a single sorbent (GAC) and used the physical non-equilibrium model described above

to simulate sorption and desorption; sorption properties (Table 1) were taken from the calibrated simulations (Figure 3).

Section 5: Results

Performance of the three PRB configurations (Figure 5) and a no-treatment reference case were simulated at three outflow rates (2.1, 3.22, and 5.0 mL/min, Q1-3, respectively). These values were chosen to produce flux rates proportional to those considered in the physical experiments (1.04 mL/min for Exp. 01, 0.70 mL/min for Exp. 02). Each simulation was run in three stages: 1) 24-hr equilibration for water flow at the target flow rate; 2) 0.1-hr solute injection at a rate of 0.83 mL/min; and 3) transport at the target flow rate for 480-hr (non-reactive) to 2960-hr (reactive). This sequence reflects the methodology used in the physical experiments described above and was shown necessary to replicate during model calibration (M.J. Nicholl personal communication). The simulation matrix (Table 3) is structured by Flow Rate (Q1, Q2, Q3), PRB configuration (A, F, W, B), and reactivity (R, N). For the PRB, Case A represents no-treatment, Case F is funnel-and-gate, Case W is staggered wells, and Case B is parallel bars. Simulations were run for both GAC ($K_d = 100$) and a non-reactive GAC ($K_d = 0$), which are labeled as R and N, respectively. For example: Q1-W-N represents a flow rate of 2.1 mL/min, staggered wells case, and non-reactive while Q2-F-R represents Flow Rate 2, funnel-and-gate case, and reactive. In total, 21 simulations were performed, with 12 as non-reactive and 9 as reactive.

Post-injection transport (Stage 3) for the non-reactive and reactive cases were simulated for 480 and 2960 hours, respectively (Table 3). Output from each transport simulation was evaluated to obtain: 1) hydraulic head (h) at the outflow node; 2) initial solute mass; and 3) outflow concentration as a function of time. Hydraulic head at the outflow node (Table 4) was principally controlled by flow rate, with PRB configuration having a lesser influence. As expected, reactivity of the treatment materials had no discernible effect on the outflow head.

Head at the upstream boundary was set at 20 cm, and varied between 19.8 and 19.5 cm at the outflow, which gives a hydraulic gradient of 0.0022 to 0.0055. At all three flow rates, head loss across the system (inlet - outlet) was 0.0-0.5% higher for the funnel-and-gate simulations than for the no-treatment option. Conversely, head loss was lower in the staggered wells (2.4-2.7%) and parallel bars (3.1-3.4%) configurations than for the no-treatment option.

Results for the transport simulations are presented in terms of the Mass Fraction Recovered (Mfr), which we define as the cumulative solute mass passed through the outflow relative to the initial mass (mg/mg). Solute recovery was virtually complete (Mfr = 1.0) in all of the non-reactive simulations (Figure 6, Table 5). The data shows that the pulse of solute passes through the funnel-and-gate faster than the other configurations at all three flow rates. The separation between the funnel-and-gate and the other three cases increases with decreasing flow rate. Under non-reactive conditions, the no-treatment, staggered wells, and parallel bars show nearly indistinguishable behavior at all three flow rates (Figure 6). In all configurations, the time for the center of mass (Mfr = 0.5) to pass through a non-reactive system increased as flow rate decreases. The Mfr vs. time relationship exhibits progressively steeper slopes as the flow rate increases (Figure 6). In all cases, the slope of the Mfr curve is smaller on the trailing edge of the solute pulse that on the leading edge; this effect decreases with increased flow rate. The time required for all of the solute (Mfr = 1.0) to exit the system was 320 hours, 210 hours, and 130 hours for flow rates Q1, Q2, and Q3, respectively.

Results for the reactive simulations (K_d = 100) are shown in Figures 7-9 and Table 6. In each graph, the non-treatment case (Figure 6) is shown for reference. All simulations were run long enough (2960 hours) to see clear differences between the cases, but stopped short of 100% recovery. Note that the Mfr curves flatten out to such a degree that the simulation time needed to

reach 100% recovery would be prohibitive. At all flow rates, the funnel-and-gate design (Q1-F-R, Q2-F-R, Q3-F-R) retarded solute to a higher degree than the other configurations. This delay decreases as flow rate increases. Simulations for the staggered wells configuration (Q1-W-R, Q2-W-R, Q3-W-R) show a gradual slope that increases rapidly before leveling off. In addition, the solute pulse both arrives earlier, and increases more rapidly than for the funnel-and-gate (Figures 7-9). The parallel bar simulations (Q1-B-R, Q2-B-R, Q3-B-R) demonstrate an early initial spike of solute (~20%) that transitions into a shallow slope. However, by the time the roughly 50% of the solute is extracted, the parallel bars appear to be more effective at removal than the staggered wells. Plotting the Mfr data as a function of outflow volume (not shown) does not collapse the curves on top of one another, showing that there is a velocity effect. The Mfr curves for the funnel-and-gate and staggered well configurations become more parabolic with increasing flow rate. For the parallel bars, the initial spike becomes larger with increasing flow rate, and the post-spike behavior becomes more parabolic.

Section 6: Discussion

The fundamental objective of this work was to evaluate the utility of bench scale sand tank experiments at assessing permeable reactive barrier design. Our criteria for meeting this goal was that differences between PRB designs could be identified solely by measuring concentration in outflow from the sand tank models. For the scenarios considered here (Figure 5), numerical simulations clearly showed that PRB design had a quantifiable effect on outflow concentration (Figure 7-9), provided that the solute reacted with the PRB materials. Conversely, use of a conservative (non-reactive) solute did not allow us to discern between PRB design alternatives (Figure 6). Employing the data collected from the numerical simulations can refine the design of the reactive barriers prior to physical sand tank experiments. The use of a reactive tracer is critical in assessing the efficacy of differing reactive barriers in a physical experiment. Analyzing reactive tracer concentration from the outflow provides real time hydraulic and solute removal data that could otherwise not be obtained without influencing the flow within the tank. Utilization of numerically simulated reactive barriers could be a way to predict and validate the use of a physical, bench-scale sand tank model.

The slow expulsion of solute over the course of 2960 hours in each of the reactive simulations is attributed to the physical non-equilibrium calibration. Concentration gradients within the GAC dictate the direction of solute flow from mobile to immobile water fractions. As the solute initially flows through the GAC, the mobile water has high solute concentration, while the immobile water has a near zero concentration. The gradient causes solute to diffuse from the mobile to the immobile water fraction, where it absorbs onto the GAC particles. This process occurs for each GAC filled-polygon along the solute flow path. Desorption is initialized by reversing the concentration gradient as clean water enters the system post solute injection. Zero

solute concentration water enters the system from the upstream boundary and enters the mobile water, causing solute to diffuse from the immobile to mobile water, desorbing from the GAC to the immobile water. As the flow rate increases, desorption occurs at a significantly higher rate due to the additional clean water pulling solute from the GAC.

Across all reactive simulations, the funnel-and-gate configurations were considerably more effective at retarding transport than the staggered wells and parallel bars designs. For Q1 (2.1 mL/min) at 2960 hours, the Mass Fraction Recovered (Mfr) or the cumulative solute mass relative to initial solute mass, at the downstream reservoir was 0.235 for the funnel-and-gate (Figure 7, Table 6), which is more than a factor of two lower than values for the staggered wells (0.694) and parallel bars (0.631). This is possibly due to focusing the solute into the large area of GAC, decreasing the effect of desorption at the lower flow rates. As flow rate increased, the efficiency of the funnel-and-gate configuration decreased relative to that of the staggered wells and parallel bars (Figure 9, Table 6). For example, at Q3 (5.0 mL/min) the Mfr for the funnel-and-gate was 0.864 at 2960 hours, which is roughly 10% less than for the staggered wells (0.958) and parallel bars (0.975). Much of this compression with increased flow rate (Q) can be explained by the well-known tailing effect, where desorption slows as concentration gradients become small (e.g., Kebria et al., 2016; Mortazavian et al., 2019). However, the funnel-and-gate also acts to increase flow velocity to a much greater degree than either of the other two configurations, which increases the rate of desorption on the trailing side of the solute pulse.

The staggered wells configuration showed strong retardation at early time (Figures 7-9), which can be attributed to overlapping of the wells, which effectively captures the entire front of the pulse. The subsequent rapid desorption compared to the other designs can be explained by the short transport path through the reactive barrier. All three barriers were designed to be 8 cm

thick (Figure 5), however, for the staggered wells, solute will likely pass through only one of the 4 cm diameter wells, thus increasing the desorption rate, or at least decreasing the opportunity for desorption to be followed by re-adsorption. The distinct spike of solute near the beginning of each parallel bar simulation is attributed to the solute plume passing between the two central bars, while the slow release of solute is driven by preferential flow into the more hydraulically conductive and porous GAC. This effect would be expected to decline with clogging of the reactive media (Flury et al., 2009; Zhong et al., 2012).

The work presented here shows that sand tank experiments can be used to bridge the gap between batch/column experiments and pilot field tests without significant cost. The performance of a PRB can be considered under quasi-realistic conditions with a bench-scale tank, noting that time may place some constraints on sediment package and flow rate used in the tank. As a result, performance tests in a sand tank can be site specific, scale models of a real system which is more readily communicated to non-specialists than the results of batch, column, or field tests. The physical and numerical models can be applied in congruence to produce hydraulic upscaling models for accurate simulations of field reactive barriers of differing designs.

The limitations of testing reactive barrier performance in sand tanks are disposal of material, time required for fabrication and runtime, and limited data collection methods. In our approach, the reactive tracer used in the physical experiments was hazardous, thus requiring the use of proper handling and disposal of 45 liters of contaminated sand and pore water per experiment. The mass of the saturated soil within the tank exhibits lateral pressures that distort the tank walls increasing the chance of failure. As a result, sand tanks are custom built, heavy, and occupy a large spatial footprint that might not fit in small laboratories. Fabrication of a sand

tank apparatus, including all external components, can consume significant time. Non-intrusive data collection from within the sand tank is challenging without the use of sensors. Extraction of water samples from within the tank may perturb the flow field, altering experimental outcomes. Sensor placement and associated wires form local heterogeneities that may divert flow, leading to preferential flow paths. As a result, outflow concentration is the least intrusive way of extracting data from within a sand tank model, and limitations associated with that approach must be taken into account.

The research presented here can be applied to further refine the design process from bench scale models to pilot field scenarios. For a given reactive barrier configuration, sand tank experiments could be employed to assess how altering the volume of reactive material or length of treatment zone impacts the outcome. Utilizing bench scale sand tanks to assess the efficacy of differing reactive materials may provide critical information prior to field installation. For example, Exp 01 (GAC) and Exp 02 (AC-PSR) revealed that for short contact times, the adsorptive properties of AC-PSR and GAC were not consistent with results obtained through batch and column tests. Such information may be critical in determining the cost-effectiveness of advanced materials, such as AC-PSR. Numerical simulations have the ability to compare reactive barrier designs and reactive materials in quick succession, such as increasing the total volume of the GAC to mimic the total absorption of AC-PSR. Possible deviations between PRB bench scale experiments, numerical simulations, and field scale prototypes introduce model, scale, and measurement effects which impact experimental outcomes (Heller et al., 2011). These effects occur due to incorrect reproduction (geometry, flow), inconsistent force ratios, and differing measurement techniques. As a result, numerical simulations often employ scaled hydraulic conductivity parameters that are capable of modeling bulk flow, but do not incorporate fine-scale

mechanics (Scheibe et al., 1998). Calibration of numerical models to perform field scale predictions is necessary to counter these inherent effects; sand tank models have potential usage as an intermediate step in the calibration process.

An inherent problem with reactive barriers in field applications is the clogging of pore space over time through biotic activity (Zhong et al., 2012) and/or the precipitation of secondary minerals (Flury et al., 2009). Micro-scale sorption processes have a small reducing effect on the hydraulic properties of the reactive materials (hydraulic conductivity, porosity) because the thickness of the adsorbed layer is thin. In contrast, biotic or abiotic materials can accumulate to substantial thickness on the grain surfaces, with consequent effects on the hydraulic and adsorptive properties of the reactive material. The hydraulic conductivity and porosity of a reactive material can be reduced significantly in a short period of time depending on coupling between the in situ hydrogeochemistry and the installed reactive materials (Wantanaphong et al., 2006). The coatings can also act to block unused sorption sites on the reactive media. As a result, incorporations such as pea gravel mixing to increase porosity, pH adjustment, large grain reactive materials, and remixing of installed reactive materials (Li et al., 2009) are all possible to evaluate in bench scale sand tank experiments. Modeling these scenarios numerically has the ability for fast and simultaneous comparison, while pilot field test results may take years to conclude at significant cost. In numerical models, the capacity to rapidly edit media properties such as hydraulic conductivity (h), porosity (n), or absorption is invaluable. Consequently, to account for clogging, these values (h, n, K_d) require calibration from physical column or sand tank experimental results that incorporate the full flow and chemical complexity of field conditions. Combining physical and numerical models may be an avenue to evaluate reactive

barrier designs to reduce clogging, resulting in increased operation time and a reduction of costs in the long term.

Conclusions

The employment of physical sand tank experiments coupled with numerical simulations provide an additional avenue for assessing reactive barrier design and materials. Bench-scale sand tanks can be used as a cost and time effective method to bridge the gap between laboratory batch and column tests and pilot field tests by enabling the study of time dependent variables in a 2- or 3-dimensional system. For the PRB designs investigated here, numerical simulations demonstrated that PRB design had a quantifiable effect on outflow concentration, provided that the solute reacted with the PRB materials. Conversely, use of a conservative solute did not allow us to discern between PRB design alternatives. Utilizing the data obtained from the numerical simulations can refine the design of the reactive barriers prior to physical sand tank experiments. Application of numerically simulated reactive barriers could be a way to predict and validate the use of a physical, bench-scale sand tank models.

Appendix A: Tables

	Units	Aquifer Sand	GAC
K_{sat}	cm/hr	72*	276*
n_e	cm^3/cm^3	0.44*	0.60*
D_L	cm	0.5^	0.5^
D_T	cm	0.1^	0.1^
K_d	cm^3/mg	n/a	100
f	n/a	n/a	0.7
α	hr^{-1}	n/a	2.0E-03

Table 1: Material parameters obtained through direct measurement (*), sensitivity analysis (^), or calibrated simulations (MJ Nicholl personal communication); K_{sat} is the saturated hydraulic conductivity; n_e is the effective porosity; D_L and D_T are the longitudinal and transverse dispersivities, respectively; K_d is the effective Langmuir sorption coefficient; f is the fraction (0-1) of potential sorption sites that are in contact with immobile water; and α describes mass transfer of solute between the mobile and immobile water fractions.

	Nodes	1D elements	2D elements
No-Treatment	6578	311	12898
Funnel-and-Gate	6811	403	13364
Staggered Wells	6485	419	12712
Parallel Bars	6628	407	12998

Table 2: Statistical characteristics of the finite element mesh by PRB configuration. Nodes are defined as intersection points (corners) of individual polygons; 1D elements are sides of a polygon that reside on a boundary of the model domain (defined by 2 nodes); and 2D elements are polygons that reside within the model domain itself (defined by 3 nodes). For each configuration, the finite element mesh was automatically generated by HYDRUS 2D/3D with the size option set to prevent the separation distance between nodes from exceeding 1.00 cm.

	Case A	Case F	Case W	Case B
Q1 = 2.1 mL/min	Q1-A-N	Q1-F-N/R	Q1-W-N/R	Q1-B-N/R
Q2 = 3.22 mL/min	Q2-A-N	Q2-F-N/R	Q2-W-N/R	Q2-B-N/R
Q3 = 5.0 mL/min	Q3-A-N	Q3-F-N/R	Q3-W-N/R	Q3-B-N/R

Table 3: Simulation matrix. Case A are the no-treatment simulations, meaning that the model domain was completely filled with the inert aquifer sand. Case F represents simulations modeling the funnel-and-gate PRB; Case W is for the staggered wells; and Case B is for the parallel bars (Figure 5). No treatment simulations are marked as –N and treatment simulations are represented as –R.

Head (cm)	Q1	Q2	Q3
No-Treatment	19.792	19.684	19.501
Funnel-and-Gate	19.791	19.683	19.501
Staggered Wells	19.797	19.692	19.514
Parallel Bars	19.799	19.694	19.518

Table 4: Hydraulic head (h) in cm at the outflow node, note that there was no difference for h between the reactive and non-reactive simulations.

Non-Reactive Simulations	Injected Solute (mg)	Q1 (Mfr)	Q2 (Mfr)	Q3 (Mfr)
No-Treatment	5.0287	5.02 (0.999)	5.04 (1.002)	5.04 (1.003)
Funnel-and-Gate	5.0052	4.89 (0.977)	4.98 (0.995)	4.99 (0.997)
Staggered Wells	4.9992	4.98 (0.996)	5.02 (1.004)	5.03 (1.006)
Parallel Bars	4.9997	4.97 (0.995)	5.00 (0.999)	5.00 (1.001)

Table 5: Cumulative solute recovery at the final time step (480 hours) for the non-reactive simulations. The mass of solute injected varies between PRB configurations, but not between flow rates. Columns Q1-Q3 contain two numbers per model: recovered solute in mg on the left and Mass Fraction Recovered (Mfr) in parenthesis on the right.

Reactive Simulations	Injected Solute (mg)	Q1 (Mfr)	Q2 (Mfr)	Q3 (Mfr)
Funnel-and-Gate	5.0052	1.18 (0.235)	2.91 (0.581)	4.32 (0.864)
Staggered Wells	4.9992	3.47 (0.694)	4.46 (0.892)	4.88 (0.975)
Parallel Bars	4.9997	3.16 (0.631)	4.23 (0.846)	4.79 (0.958)

Table 6: Cumulative solute recovery at the final time step (2960 hours) for the reactive simulations. Columns Q1-Q3 contain two numbers per model: recovered solute in mg on the left and Mass Fraction Recovered (Mfr) in parenthesis on the right. In most cases, simulations would need to have been run for a much longer time to completely flush the system.

Appendix B: Figures

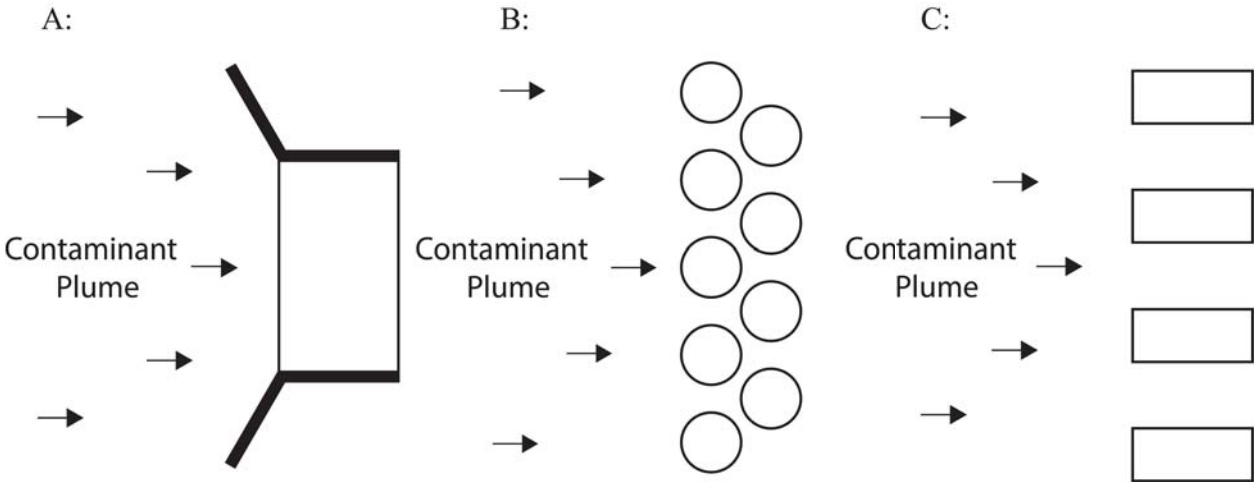

Figure 1: Map view of three PRB configurations; open circles and open rectangles would be filled with reactive material. A) Funnel-and-gate. Black polygons represent impermeable material, designed to direct (funnel) flow into the rectangular gate. B) Staggered wells. C) Parallel bars.

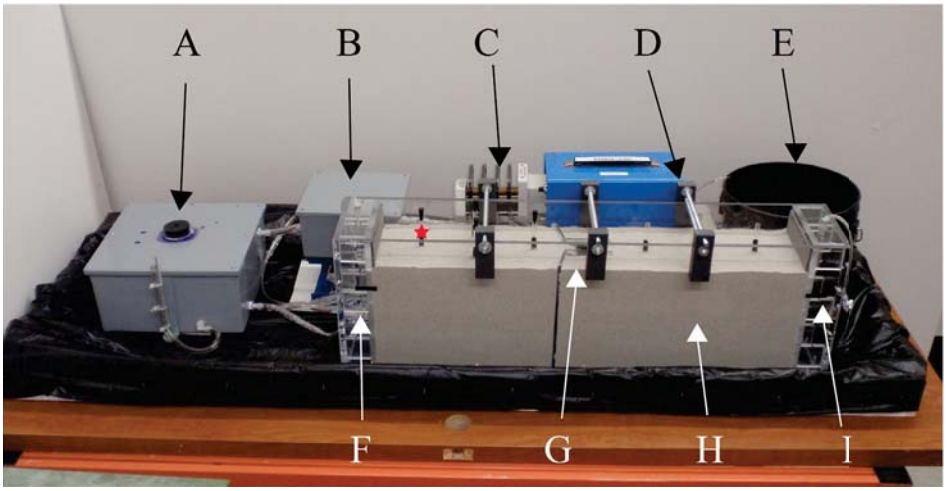

Figure 2: Bench-scale sand tank experiment with supporting apparatus enclosed by a containment tray. The red star represents the Cr(VI) injection point (well) for Exp. 01 and Exp. 02. A: fluid supply tank, B: constant head source, C: peristaltic pump, D: anti-deflection clamps, E: outflow reservoir, F: upstream reservoir, G: funnel-and-gate, H: quartz sand sediment package, I: downstream reservoir.

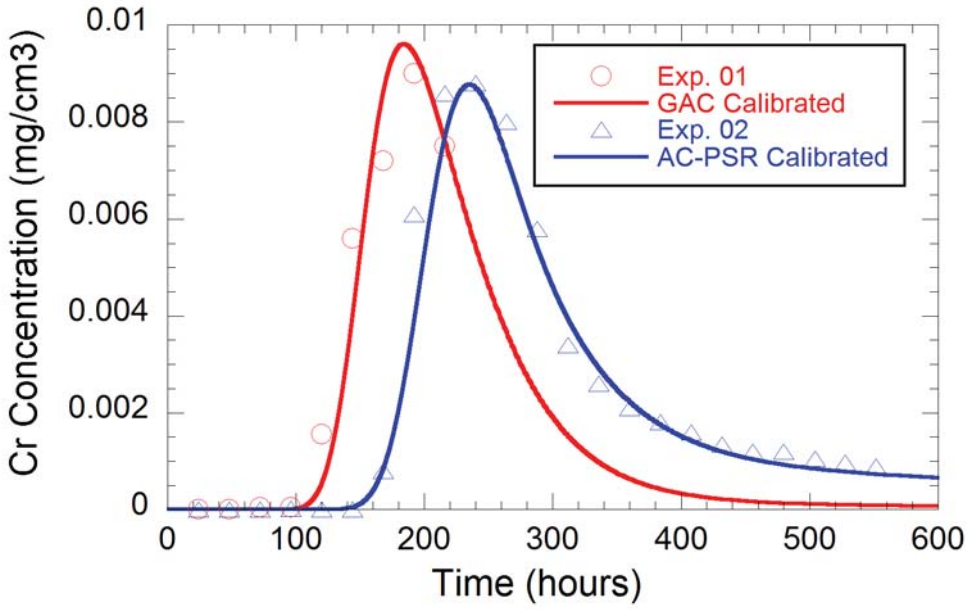

Figure 3: Measured Cr(VI) concentrations from the outflow of Exp. 01 (1.04 mL/min, 216 hours) and Exp. 02 (0.70 mL/min, 552 hours) are shown with calibrated numerical simulations (MJ Nicholl personal communication).

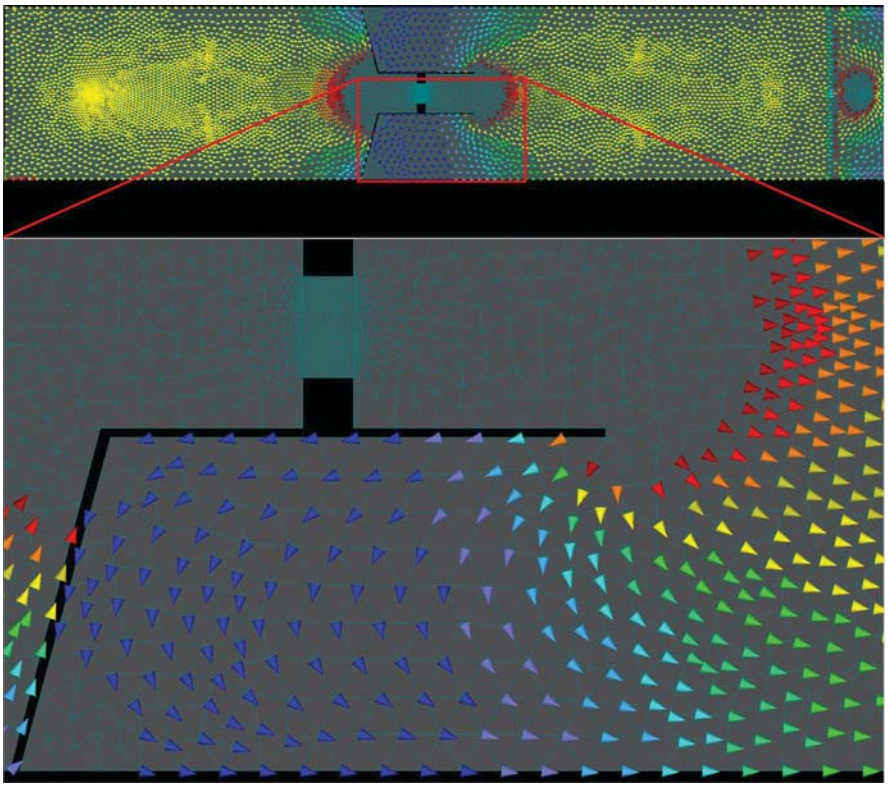

Figure 4: Vector velocity map of numerical simulations from Exp. 01 and Exp. 02 displaying the counter current and no flow zone. Arrow colors represent a gradient of velocities from high (red, 0.250 cm/sec) to low (blue, ~0.0 cm/sec). Nodes without arrows indicate flow rates not within the defined bracket of 0.0 to 0.250 cm/sec.

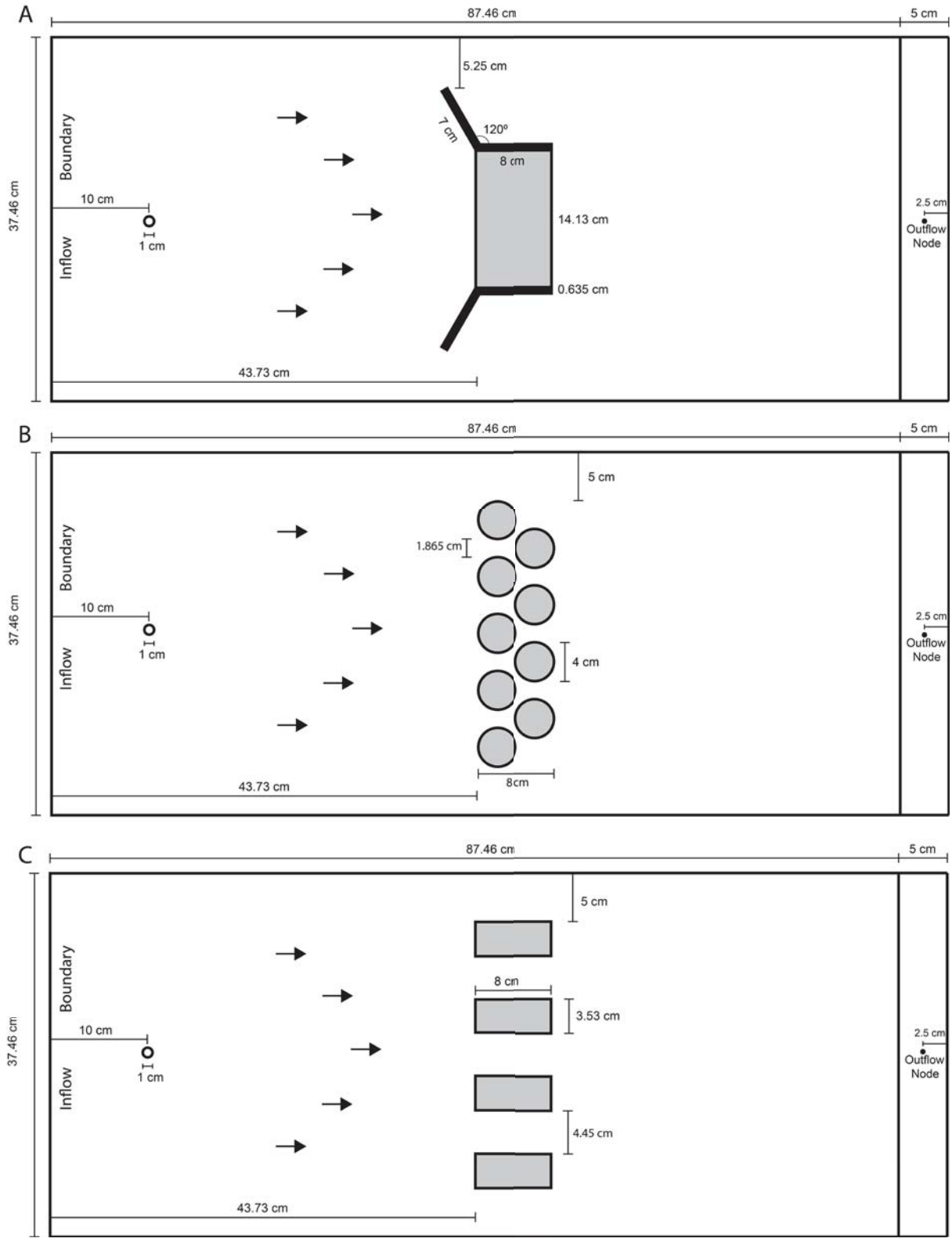

Figure 5: Map view of the simulation domains: A) funnel-and-gate (F); B) staggered wells (W); and C) parallel bars (B). Black filled polygons (funnel-and-gate domain) represent impermeable material. Grey filled circles and polygons represent treatment zones (GAC).

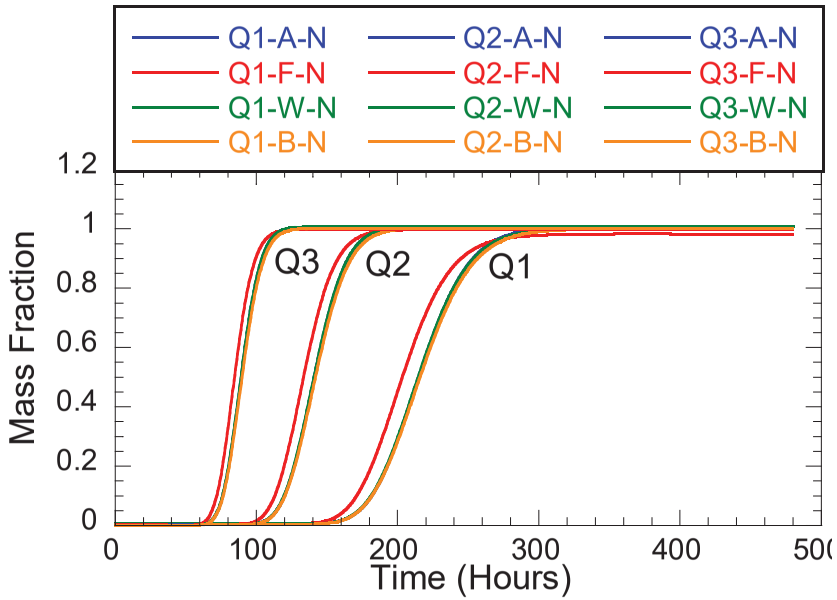

Figure 6: Model results for non-reactive simulations as a function of mass fraction.

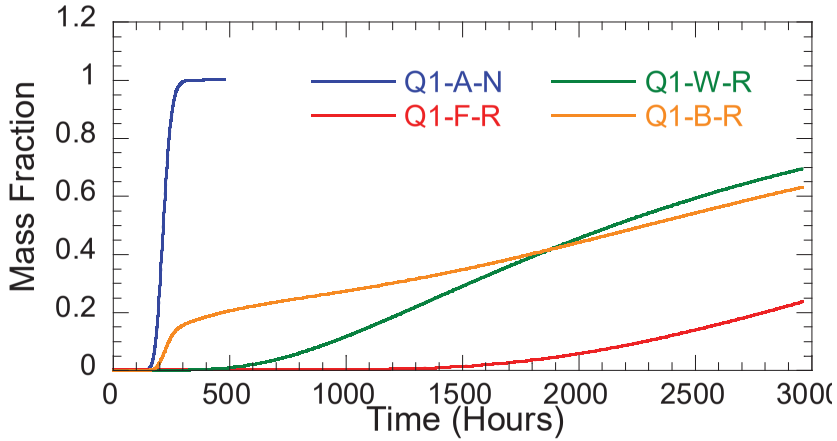

Figure 7: Model results for Q1 (2.1 mL/min) as a function of mass fraction.

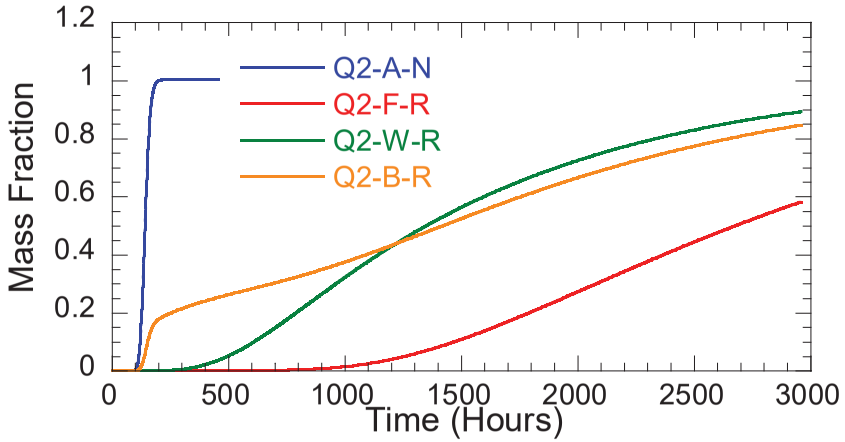

Figure 8: Model results for Q2 (3.22 mL/min) as a function of mass fraction.

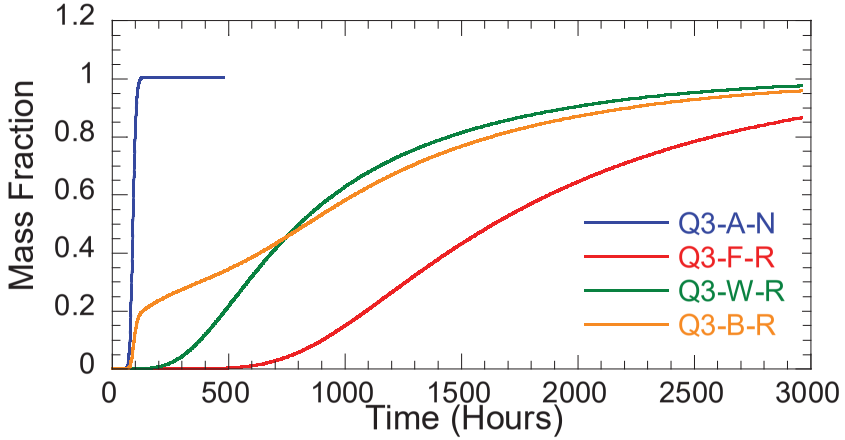

Figure 9: Model results for Q3 (5.0 mL/min) as a function of mass fraction.

References

Babel, S., & Kurniawan, T. (2003, 2 28). Low-cost adsorbents for heavy metals uptake from contaminated water: a review. *Journal of hazardous materials, 97*(1-3), 219-43.

Barth, G., Hill, M., & Illangasekare, T. (2001). Predictive modeling of flow and transport in a two-dimensional intermediate-scale, heterogeneous porous medium. *Water Resources ….*

Blowes, D., Ptacek, C., Benner, S., McRae, C., & Puls, R. (1998). Treatment of dissolved metals using permeable reactive barriers. *IAHS-AISH Publication*.

Blowes, D., Ptacek, C., Benner, S., McRae, C., Bennett, T., & Puls, R. (2000). Treatment of inorganic contaminants using permeable reactive barriers. *Journal of Contaminant Hydrology*.

Chorover J., Brusseau M. (2008) Kinetics of Sorption—Desorption. In: Brantley S., Kubicki J., White A. (eds) *Kinetics of Water-Rock Interaction*. Springer, New York, NY

Das, D. (2002). Hydrodynamic modelling for groundwater flow through permeable reactive barriers. *Hydrological Processes*.

Day, S., O'Hannesin, S., & Marsden, L. (1999). Geotechnical techniques for the construction of reactive barriers. *Journal of Hazardous Materials*.

Flury, B., Eggenberger, U., & Mäder, U. (2009, 4). First results of operating and monitoring an innovative design of a permeable reactive barrier for the remediation of chromate contaminated groundwater. *Applied Geochemistry, 24*(4), 687-696.

Gavaskar, A. (1999). Design and construction techniques for permeable reactive barriers. *Journal of Hazardous Materials*.

Gibert, O., Pomierny, S., Rowe, I., & Kalin, R. (2008). Selection of organic substrates as potential reactive materials for use in a denitrification permeable reactive barrier (PRB). *Bioresource Technology*.

Gupta, N., & Fox, T. (1999). Hydrogeologic modeling for permeable reactive barriers. *Journal of Hazardous Materials*.

Heller, V. (2011, 6). Scale effects in physical hydraulic engineering models. *Journal of Hydraulic Research, 49*(3), 293-306.

Higgins, M., & Olson, T. (2009). Life-cycle case study comparison of permeable reactive barrier versus pump-and-treat remediation. *Environmental Science and Technology*.

Hudak, P. (2008). Evaluation of reactive well networks for remediating heterogeneous aquifers. *Journal of Environmental Science and Health - Part A Toxic/Hazardous Substances and Environmental Engineering*.

Jeen, S., Gillham, R., & Przepiora, A. (2011). Predictions of long-term performance of granular iron permeable reactive barriers: Field-scale evaluation. *Journal of Contaminant Hydrology*.

Kanel, S., Greneche, J., & Choi, H. (2006). Arsenic(V) removal from groundwater using nano scale zero-valent iron as a colloidal reactive barrier material. *Environmental Science and Technology*.

Kebria, D., Taghizadeh, M., Camacho, J., & Latifi, N. (2016). Remediation of PCE contaminated clay soil by coupling electrokinetics with zero-valent iron permeable reactive barrier. *Environmental Earth Sciences*.

Klammler, H., & Hatfield, K. (2008). Analytical solutions for flow fields near continuous wall reactive barriers. *Journal of Contaminant Hydrology*.

Kornilovych, B., Wireman, M., Ubaldini, S., Guglietta, D., Koshik, Y., Caruso, B., & Kovalchuk, I. (2018). Uranium Removal from Groundwater by Permeable Reactive Barrier with Zero-Valent Iron and Organic Carbon Mixtures: Laboratory and Field Studies. *Metals*.

Krüger, O., Kalbe, U., Berger, W., Simon, F., & Meza, S. (2012). Leaching experiments on the release of heavy metals and PAH from soil and waste materials. *Journal of Hazardous Materials*.

Lee, S., Kim, M., Kim, D., & Lee, Y. (2014). Fate and transport of zinc in a sand tank model: Monitoring of 2-D plume using TDR method. *Environmental Earth Sciences*.

Li, L., & Benson, C. (2010, 9). Evaluation of five strategies to limit the impact of fouling in permeable reactive barriers. *Journal of Hazardous Materials, 181*(1-3), 170-180.

Li, L., Quinlivan, P., & Knappe, D. (2002). Effects of activated carbon surface chemistry and pore structure on the adsorption of organic contaminants from aqueous solution. *Carbon, 40*(12), 2085-2100.

Liu, S., Yeh, T.-C., & Gardiner, R. (2002). Effectiveness of hydraulic tomography: Sandbox experiments. *Water Resources Research*.

Luo, X., Liu, H., Huang, G., Li, Y., Zhao, Y., & Li, X. (2016). Remediation of arsenic-contaminated groundwater using media-injected permeable reactive barriers with a modified montmorillonite: sand tank studies. *Environmental Science and Pollution Research*.

Mao, D., Revil, A., Hort, R., Munakata-Marr, J., Atekwana, E., & Kulessa, B. (2015). Resistivity and self-potential tomography applied to groundwater remediation and contaminant plumes: Sandbox and field experiments. *Journal of Hydrology*.

Mayer, K., Blowes, D., & Frind, E. (2001). Reactive transport modeling of an in situ reactive barrier for the treatment of hexavalent chromium and trichloroethylene in groundwater. *Water Resources Research*.

Mortazavian, S., Saber, A., Hong, J., Bae, J., Chun, D., Wong, N., . . . Moon, J. (2019, 1 25). Synthesis, characterization, and kinetic study of activated carbon modified by polysulfide rubber coating for aqueous hexavalent chromium removal. *Journal of Industrial and Engineering Chemistry, 69*, 196-210.

Obiri-Nyarko, F., Grajales-Mesa, S., & Malina, G. (2014). An overview of permeable reactive barriers for in situ sustainable groundwater remediation. *Chemosphere*.

Phillips, D., Nooten, T., Bastiaens, L., Russell, M., Dickson, K., Plant, S., . . . Kalin, R. (2010). Ten year performance evaluation of a field-scale zero-valent iron permeable reactive barrier installed to remediate trichloroethene contaminated groundwater. *Environmental Science and Technology*.

Powell, R., Puls, R., Blowes, D., Vogan, J., Gillham, R., Powell, P., . . . Landis, R. (1998). *Permeable Reactive Barrier Technologies for Contaminant Remediation.*

Ruiz, C., Mena, E., Cañizares, P., Villaseñor, J., & Rodrigo, M. (2014). Removal of 2,4,6-trichlorophenol from spiked clay soils by electrokinetic soil flushing assisted with granular activated carbon permeable reactive barrier. *Industrial and Engineering Chemistry Research*.

Scheibe, T., & Yabusaki, S. (1998, 11). Scaling of flow and transport behavior in heterogeneous groundwater systems. *Advances in Water Resources, 22*(3), 223-238.

Šimůnek, J., & van Genuchten, M. (2008). Modeling Nonequilibrium Flow and Transport Processes Using HYDRUS. *Vadose Zone Journal*.

Simunek, J., Van Genuchten, M., & Sejna, M. (2011). The HYDRUS Software Package for Simulating the Two- and Three-Dimensions Movement of Water, Heat, and Multiple Solutes in Variably-Saturated Media. *Technical Manual*.

The Finite Element Method. (1980). *Mathematics in Science and Engineering*.

Truax, D., Britto, R., & Sherrard, J. (1995). Bench-scale studies of reactor-based treatment of fuel-contaminated soils. *Waste Management, 15*(5-6), 351-357.

Ursino, N., Gimmi, T., & Flühler, H. (2001). Combined effects of heterogeneity, anisotropy, and saturation on steady state flow and transport: A laboratory sand tank experiment. *Water Resources Research*.

Vogan, J., Focht, R., Clark, D., & Graham, S. (1999). Performance evaluation of a permeable reactive barrier for remediation of dissolved chlorinated solvents in groundwater. *Journal of Hazardous Materials*.

Wantanaphong, J., Mooney, S., & Bailey, E. (2006, 8 10). Quantification of pore clogging characteristics in potential permeable reactive barrier (PRB) substrates using image analysis. *Journal of Contaminant Hydrology, 86*(3-4), 299-320.

Waybrant, K., Ptacek, C., & Blowes, D. (2002). Treatment of mine drainage using permeable reactive barriers: Column experiments. *Environmental Science and Technology*.

Weisener, C., Sale, K., Smyth, D., & Blowes, D. (2005). Field column study using zerovalent iron for mercury removal from contaminated groundwater. *Environmental Science and Technology*.

Zhong, X., & Wu, Y. (2013). Bioclogging in porous media under continuous-flow condition. *Environmental Earth Sciences, 68*(8), 2417-2425.

Curriculum Vitae

Brandon Meier, M.S.

Email Address: brandon.meierb4@gmail.com

Education:

University of Nevada, Las Vegas
M.S., Hydrology, December 2019
B.S., Geology, December 2015